Journal of Alloys and Compounds 656 (2016) 470–475

Contents lists available at ScienceDirect

Journal of Alloys and Compounds

journal homepage: http://www.elsevier.com/locate/jalcom

New low-dielectric-loss $NiZrNb_2O_8$ ceramics for microwave application

Wang-Suo Xia [a, *], Fan-Yu Yang [b], Guo-Ying Zhang [a], Kui Han [a], De-chun Guo [b]

[a] College of Science, China University of Mining and Technology, Xuzhou 221008, China
[b] School of Information and Electronics, Beijing Institute of Technology, Beijing 100081, China

ARTICLE INFO

Article history:
Received 9 November 2014
Received in revised form
19 September 2015
Accepted 1 October 2015

Keywords:
Ceramics
Microwave dielectric properties
Microstructure
Packing fraction
$NiZrNb_2O_8$

ABSTRACT

New low-loss $NiZrNb_2O_8$ microwave dielectric ceramics were synthesized via conventional mixed oxide route. The morphology, crystal structure and microwave dielectric properties were investigated. It exhibited a monoclinic wolframite crystal structure, with the space group of *P2/c* (C_{2h}^4). The lattice energy was carried out to evaluate the structural stability and sintering characteristics. Two kinds of grain shapes in dense samples, with similar elements ratios, were observed. Variations in the dielectric constant (ε_r) were analyzed by relative density and porosity-corrected polarizability. The quality factor ($Q \times f$) was correlated with packing fraction and grain growth. The temperature coefficient of resonant (τ_f) was depended on the dielectric constant. The typical microwave dielectric properties of $NiZrNb_2O_8$ were $\varepsilon_r = 23.77$, $Q \times f = 40280$ GHz, $\tau_f = -27.5$ ppm/°C, sintered at 1200 °C.

1. Introduction

Microwave dielectric ceramics play an important role in the development of wireless communications devices, such as global positioning systems (GPS), microwave transmitting circuits, cell phones, and intelligent transportation systems (ITS) [1]. Recent revolution in telecommunications requires developing a variety of microwave dielectric ceramics [2,3]. Dielectric ceramics have been regarded as the basic materials in modern communication technology, for those in microwave application, three requirements need to be satisfied: (1) high dielectric constant for miniaturization ($\lambda = \lambda_0/\sqrt{\varepsilon_r}$, λ is the wavelength of electromagnetic wave in dielectric material and λ_0 is the wavelength of electromagnetic wave in free space), (2) low dielectric loss (or high quality factor) for enhancing the signal-to-noise ratio, (3) the near-zero temperature coefficient of resonant frequency for good performance of the devices under different atmospheric conditions.

Ceramics of $ABNb_2O_8$ form have attracted a great deal of interests for their predominant microwave dielectric properties. Numerous investigations have been reported on $ATiNb_2O_8$with different cations substituted at A-site [4–7]. Recently, much attention has been paid to investigations on Ti-site substitution of these compositions [8–12]. Liao et al. reported that the microwave dielectric properties of $ZnZrNb_2O_8$ ceramics were dependent on the relative density [9]. Then, Cheng et al. reported the $MgZrNb_2O_8$ ceramics with high $Q \times f$ values [10]. Especially, Ramarao et al., reported a class of $AZrNb_2O_8$ (A = Mn, Mg, Zn and Co) materials last year [11]. However, it was noted that the $NiZrNb_2O_8$ had been ignored out of the $AZrNb_2O_8$ system. Furthermore, the Ni ion was an important member in bivalent ions, which was frequently used as a substitution [13–15].

In the present study, we reported the microwave dielectric properties of $NiZrNb_2O_8$ ceramics, which exhibited the same crystal structure with $AZrNb_2O_8$ (A = Mn, Mg, Zn and Co) ceramics. The $NiZrNb_2O_8$ possessed promising microwave dielectric properties ($\varepsilon_r = 23.77$, $Q \times f = 40280$ GHz, $\tau_f = -27.5$ ppm/°C) and low sintering temperature ($T_s = 1200$ °C) in $AZrNb_2O_8$ system.

2. Experimental procedure

$NiZrNb_2O_8$ ceramics were synthesized using mixed oxide route from the raw materials including NiO (98%), ZrO_2 (99%) and Nb_2O_5 (99.5%). These oxides were mixed through de-ionized water and zirconia balls for 24 h. The mixture was dried, crushed and sieved with a 40 mesh screen. Then the powders were calcined at 900 °C for 3 h in air. The calcined powders were afterwards milled for 24 h.

* Corresponding author.
E-mail address: xiaws@cumt.edu.cn (W.-S. Xia).

http://dx.doi.org/10.1016/j.jallcom.2015.10.008
0925-8388/

After drying, the powders were pressed into pellets with 10 mm in diameter and 5 mm in thickness. These pellets were then sintered at the temperature range of 1125–1250 °C for 6 h with a heating rate of 5 °C/min.

The crystal structures of the sintered samples were confirmed by analyzing powder's X-ray diffraction (XRD) patterns using a Rigaku diffractometer (Model D/Max-B, Rigaku Co., Japan) with Ni filtered Cu Kα radiation (λ = 0.1542 nm) at settings of 40 kV and 40 mA. The microstructure observation on ceramic surfaces was performed and analyzed by a scanning electron microscopy (SEM, FEI Quanta 250, USA), and the compositions of the ceramics were characterized by Energy Dispersive Spectrometer (EDS, Bruker Quantax400-10, Germany). Microwave dielectric properties of the sintered pellets were measured by a network analyzer (N5234A, Agilent Co., USA) in the frequency range of 7–8 GHz using Hakki–Coleman's dielectric resonator method [16,17]. The temperature coefficient of resonant frequency was obtained by measuring the $TE_{01\delta}$ resonant frequency from 25 °C to 85 °C. The τ_f (ppm/°C) could be calculated by noting the change in resonant frequency (Δf)

$$\tau_f = \frac{f_2 - f_1}{f_1(T_2 - T_1)} \tag{1}$$

where f_1 was resonant frequency at T_1 and f_2 was the resonant frequency at T_2.

The theoretical density and relative density were calculated by Eqs. (2) and (3):

$$\rho_{theory} = \frac{nA}{V_c N_A} \tag{2}$$

$$\rho_{relative} = \frac{\rho_{bulk}}{\rho_{theory}} \tag{3}$$

where n was the number of atoms in unit cell, A was atomic weight, V_c was unit-cell volume, and N_A was Avogadro number.

The packing fraction, defined as the summation of the volume of packed ions over the volume of a primitive unit cell, was calculated from Eq. (4) [18]:

$$\text{Packing fraction (\%)} = \frac{\text{volume of the atoms in the cell}}{\text{volume of primitive unit cell}} = \frac{\text{volume of the atoms in the cell}}{\text{volume of unit cell}} \times Z \tag{4}$$

where Z was the number of formula units per unit-cell.

3. Result and discussion

The XRD patterns of $NiZrNb_2O_8$ samples sintered at 1125–1250 °C were shown in Fig. 1. All the diffraction patterns were indexed with a wolframite structure belonged to $P2/c$ (C_{2h}^4) space group (monoclinic: ICDD-PDF #48-0327). The crystal phase of the samples with various sintering temperature exhibited no phase difference, with no second phase being detected. The Rietveld refinement analysis of $NiZrNb_2O_8$ ceramics sintered at 1200 °C was shown in Fig. 2. Moreover, as the results showed in Fig 3, the unit-cell volume of the samples decreased with an increase of the sintering temperature, and then increased when the sintering temperature was greater than 1200 °C. Furthermore, the details of peak shift with different sintering temperature were also showed in Fig. 3. The peak positions shifted to the higher angle when the sintering temperature increased from 1125 °C to 1200 °C and then shifted to the lower angle, which owed to the variation of unit-cell

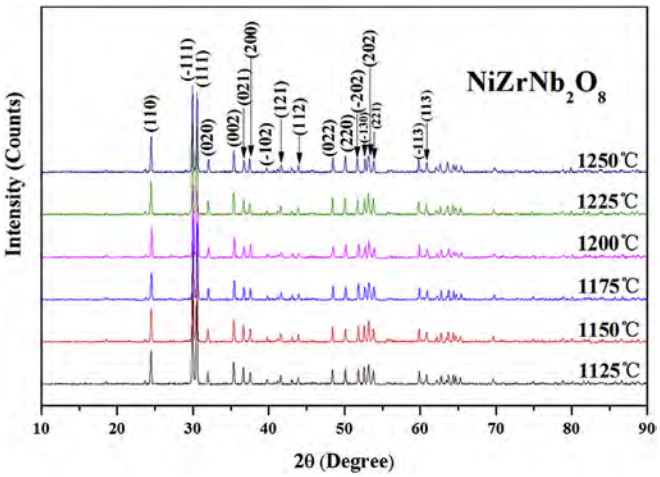

Fig. 1. The X-ray diffraction patterns of $NiZrNb_2O_8$ ceramics sintered at different sintering temperatures.

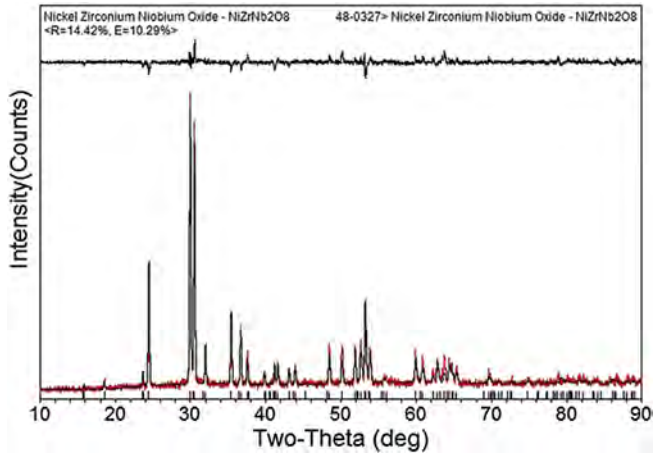

Fig. 2. The observed and calculated X-ray diffraction patterns by Rietveld analysis for $NiZrNb_2O_8$ ceramics sintered at 1200 °C.

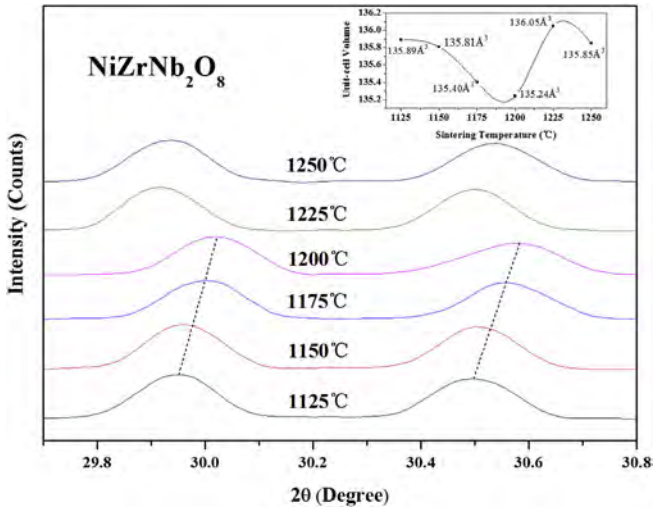

Fig. 3. Shift of X-ray diffraction peaks and unit-cell volumes of $NiZrNb_2O_8$ ceramics sintered at different sintering temperatures.

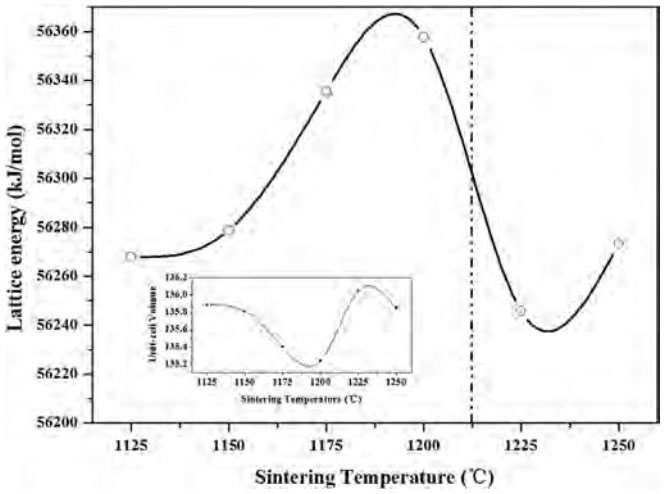

Fig. 4. Lattice energy of $NiZrNb_2O_8$ ceramics sintered at different sintering temperatures.

volume. To sum up, it was indicated in Figs. 1–3 that the phase composition was single, but the lattice parameters varied regularly when the sintering temperature was changed.

The lattice energy (U) was carried out to evaluate the structural stability of $NiZrNb_2O_8$ ceramics at different sintering temperatures. For complex ionic crystals, the lattice energy was calculated as follows [19]:

$$U = AI(2I/V_m)^{1/3} \tag{5}$$

$$2I = \sum_i n_i Z_i^2 \tag{6}$$

$$V_m = V_{cell}/Z \tag{7}$$

where I was the ionic strength, n_i was the number of ions with integer charge Z_i, the summation was taken over all the types of ions in the formula unit. V_m and V_{cell} was the molecular volume and unit-cell volume respectively. Z was the number of formula units per unit cell. Fig. 4 showed the lattice energy and the unit-cell

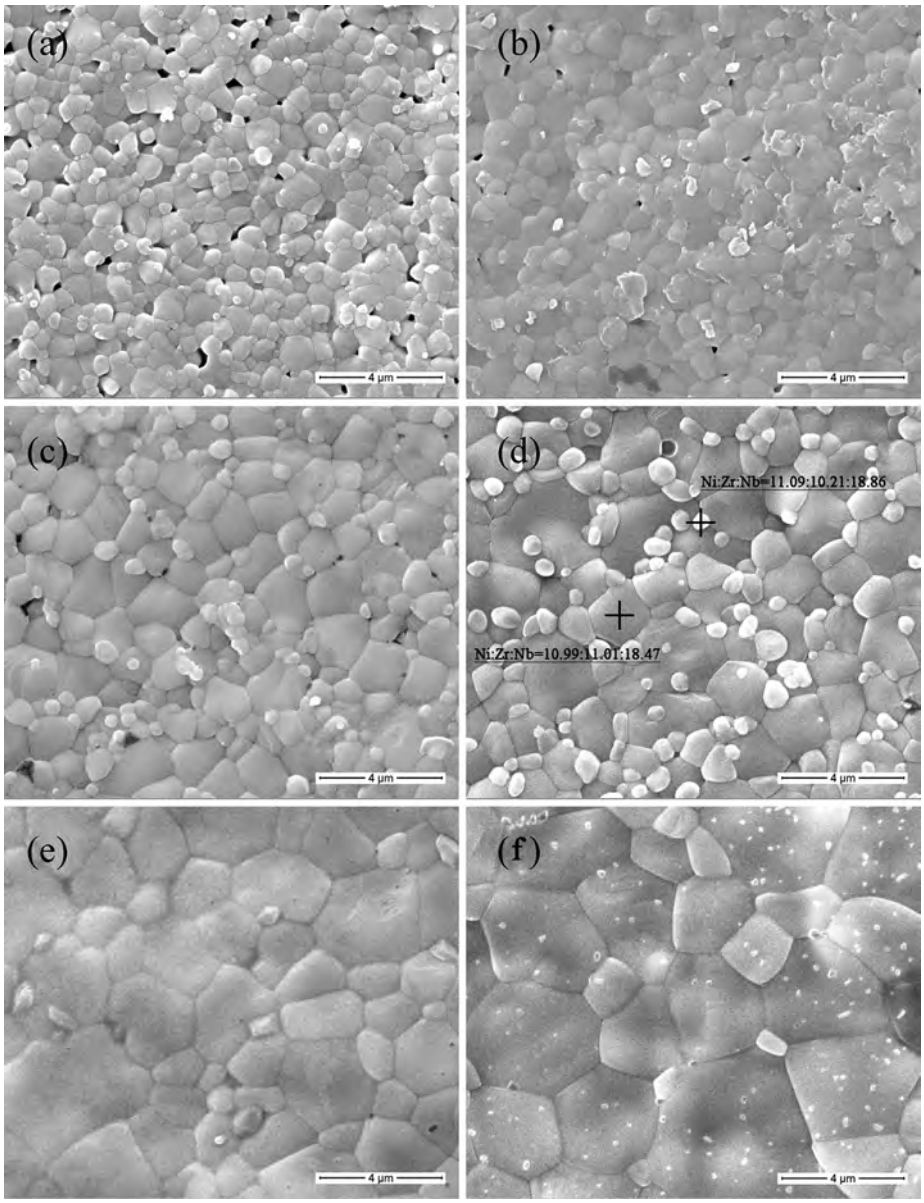

Fig. 5. Micrographs of $NiZrNb_2O_8$ ceramics sintered at (a) 1125 °C, (b) 1150 °C, (c) 1175 °C, (d) 1200 °C, (e) 1225 °C, (f) 1250 °C.

Table 1
Theory density, Apparent density, Relative density, resonant frequency (f_0), ε_r and ε_{rc} of $NiZrNb_2O_8$ ceramics.

Sintering temperature (°C)	Theory density (g/cm^3)	Apparent density (g/cm^3)	Relative density (%)	f_0 (GHz)	ε_r	ε_{rc}
1125	5.6663	5.4840	96.78	7.66	24.01	25.15
1150	5.6697	5.5657	98.17	7.58	24.27	24.91
1175	5.6869	5.5909	98.31	7.58	24.25	24.84
1200	5.6936	5.5336	97.19	7.59	23.77	24.75
1225	5.6595	5.5307	97.72	7.67	23.86	24.65
1250	5.6679	5.5138	97.28	7.67	23.61	24.55

volume (the illustration bellow) of $NiZrNb_2O_8$ ceramics sintered at 1125–1250 °C for 6 h. It was noted that the tendency between lattice energy and unit-cell volume was opposite, suggesting that the structural stability could be predicted in sintering process. The lattice energy of $NiZrNb_2O_8$ ceramics increased to maximum (56357.78 kJ/mol) at 1200 °C, and then decreased. Noticeably, it indicated that the $NiZrNb_2O_8$ ceramics with the most stable structure was obtained at 1200 °C, which was lower than other bivalent-ion compounds in the $AZrNb_2O_8$ ceramic system [10,11].

Fig. 5 illustrated the SEM images of $NiZrNb_2O_8$ ceramics sintered at 1125–1250 °C for 6 h. In all images, two kinds of grain shapes were observed. And the grain size increased with the increasing sintering temperature. It also suggested that the well-developed microstructure was observed at 1200 °C as shown in Fig. 3(d). In order to confirm the chemical composition of the two kinds of shapes, the elemental analysis for marked spots at $NiZrNb_2O_8$ ceramics was carried out in Fig. 3(d). The EDS results implied that the two kinds of grains had the same element composition.

The calculated results of theory density, relative density, ε_r and porosity-corrected permittivity (ε_{rc}), together with the measured results of apparent density, were all listed in Table 1. As shown in Table 1, the apparent densities of all samples were more than 95% of their theoretical densities. As the sintering temperature increased, the dielectric constant increased at first and then slightly decreased. The variation tendency of the ε_r values was similar with that of the relative densities, owing to the lower porosity. The porosity-corrected permittivity (ε_{rc}) was calculated as follows [20]:

$$\frac{\varepsilon_r - \varepsilon_{rc}}{3\varepsilon_r} = \frac{\delta(\varepsilon_1 - \varepsilon_{rc})}{\varepsilon_1 + 2\varepsilon_r} \tag{8}$$

where ε_r was the measured dielectric constant, ε_1 was dielectric constant of porosity, δ was the fractional porosity. It was known that the dielectric constant of microwave ceramics was dependent on ionic polarizability. The relationship between polarizability and dielectric constant could be expressed by the Clausius–Mosotti equation [21]:

$$\alpha = \frac{3V_m}{4\pi} \cdot \frac{K-1}{K+2} \tag{9}$$

where V_m was the molar volume, K was the real part of the complex dielectric constant. The variation of the porosity-corrected polarizability (α_c) with the change of sintering temperature has been shown in Fig. 6. It was noted that the variation of α_c was consisted

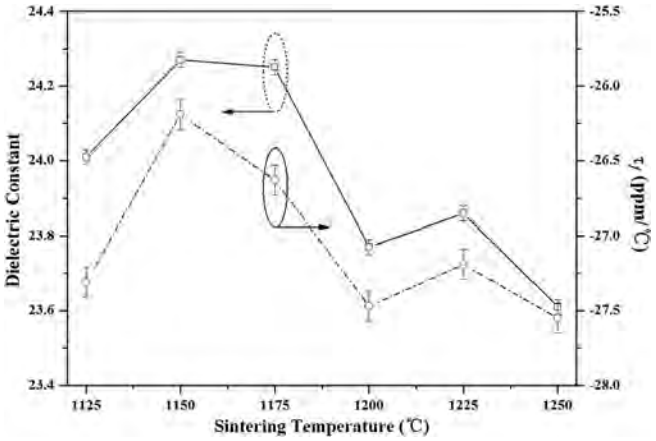

Fig. 7. Relation between dielectric constant and τ_f values of $NiZrNb_2O_8$ ceramics sintered at different sintering temperatures.

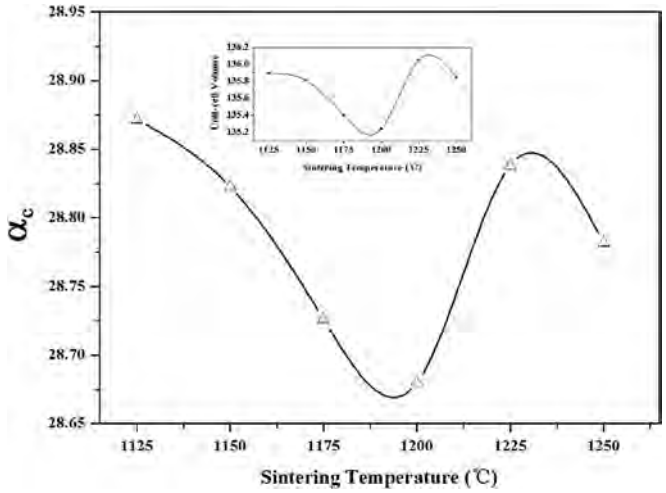

Fig. 6. The porosity-corrected polarizability of $NiZrNb_2O_8$ ceramics sintered at different sintering temperatures.

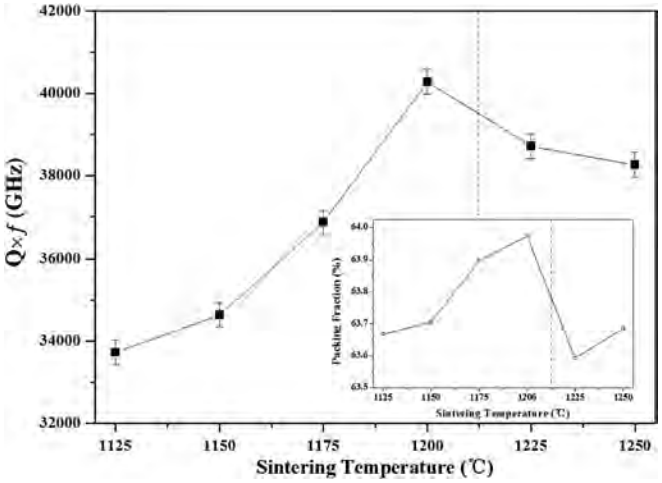

Fig. 8. Variation in Q × f values and packing fraction of $NiZrNb_2O_8$ ceramics sintered at different sintering temperatures.

Table 2
Sintering temperature, relative density, α_c, packing fraction and microwave dielectric properties of $AZrNb_2O_8$ ceramics.

A	Sintering temperature (°C)	Relative density (%)	ε_r	α_c (Å^3)	Q × f (GHz)	Packing fraction (%)	τ_f (ppm/°C)	
Ni	1200	97.2	23.77	28.68	40,280	63.97	−27.5	This work
Co	1300	94.2	12.3	26.35	26,950	65.00	−28.2	Ref. [9]
Mg	1500	94.8	9.60	24.86	58,500	65.05	−31.5	Ref. [9]
Zn	1350	95.4	16.5	28.07	53,450	64.65	−49.8	Ref. [9]
Mn	1400	93.7	16.7	28.82	40,700	63.84	−29.6	Ref. [9]

with that of unit-cell volume, which implied that the molecular polarizability of $NiZrNb_2O_8$ ceramics was strongly affected by the unit-cell volume.

Fig. 7 showed the correlation between τ_f and dielectric constant. As shown in Fig. 7, the change rule of τ_f and dielectric constant was consistent. It was known that τ_f was depended on the temperature coefficient of permittivity (τ_ε) and the linear thermal expansion coefficient (α_L), expressed in Eq. (10):

$$\tau_f = -\left(\frac{\tau_\varepsilon}{2} + \alpha_L\right) \tag{10}$$

According to the research of Harrop [22], the relationship between ε and τ_ε was founded as follows:

$$\tau_\varepsilon = -\alpha_L \varepsilon \tag{11}$$

Based on Eqs. (10) and (11), the correlation between τ_f and ε was obtained:

$$\tau_f = \alpha_L \times \left(\frac{\varepsilon}{2} - 1\right) \propto \varepsilon \tag{12}$$

Fig. 8 showed the Q × f values of the $NiZrNb_2O_8$ ceramics sintered at 1125–1250 °C for 6 h. As shown in Fig. 8, the Q × f values firstly increased from 33,730 GHz to 40,280 GHz and then slightly decreased. The quality factor of ceramics at microwave frequency was governed not only by extrinsic parameters such as porosity, density, grain size and phase composition, but also by intrinsic parameters related to lattice anharmonicity such as the packing fraction and the nature of bonding [18,23]. According to the analysis of density and XRD results, all the samples possessed high-density and single-phase nature. Kim et al. reported the relationship between the quality factor and the atomic packing fraction [18]. In order to explain the variation of the quality factor, the packing fraction was calculated according to Eq. (4), which was also shown in Fig. 8. As the results of Fig. 8 showed, the sample with a higher packing fraction, which was sintered at 1125–1200 °C, exhibited a higher Q × f value. However, it was important to note that the variation trend of Q × f value and packing fraction was not quite the same. Based on the results of SEM images, the grain size showed an increasing trend with the increase of sintering temperature, which was another reason for the increase of the Q × f values. In combination with the analysis of grain growth, the Q × f values increased to maximum value and thereafter decreased, as the increasing sintering temperature. The results suggested that the Q × f values of $NiZrNb_2O_8$ ceramics were depended on the packing fraction and grain growth.

The microwave dielectric properties of $AZrNb_2O_8$ (A = Ni, Co, Mg, Zn and Mn) ceramics were illustrated in Table 2. In comparison, the microwave dielectric properties of $NiZrNb_2O_8$ ceramics, especially dielectric constant and sintering temperature, were better than other bivalent-ion compounds in the $AZrNb_2O_8$ ceramic system. As shown in Table 2, the dielectric constant of $NiZrNb_2O_8$ ceramics was 23.77, which was bigger than those of $AZrNb_2O_8$ (A = Co, Mg, Zn and Mn) ceramics, owing to the higher relative density and bigger porosity-corrected polarizability. In addition, the Q × f values of $AZrNb_2O_8$ (A = Ni, Co, Mg, Zn and Mn) ceramics were dependent on the packing fraction, except for $NiZrNb_2O_8$ and $CoZrNb_2O_8$. The anomalous behaviors of $NiZrNb_2O_8$ and $CoZrNb_2O_8$ ceramics were owing to the existence of electrons in 3*d* orbit [11].

4. Conclusion

New low-dielectric-loss $NiZrNb_2O_8$ ceramics were prepared by solid-state reaction and observed to possess a single-phase nature with a monoclinic wolframite structure belonged to *P2/c* (C_{2h}^4) space group. Lattice energy was carried out to evaluate the structural stability of $NiZrNb_2O_8$ ceramics. The surface structure of dense samples exhibited two kinds of grain shapes with the similar chemical composition. The promising microwave dielectric properties were ε_r = 23.77, Q × f = 40280 GHz, τ_f = −27.5 ppm/°C, sintered at 1200 °C. The relative density and porosity-corrected polarizability were then calculated to evaluate the dielectric constant. The Q × f values were dominated by the packing fraction and grain growth. The τ_f values were correlated with the dielectric constant.

Acknowledgments

This work is supported by the projects from the Fundamental Research Funds for the Central Universities of China University of Mining and Technology under Grant No. 2014QNA69 and the National Natural Science Foundation of China under Grant No. 51402353.

References

[1] I.M. Reaney, D. Iddles, Microwave dielectric ceramics for resonators and filters in mobile phone networks, J. Am. Ceram. Soc. 89 (2006) 2063–2072.
[2] D. Zhou, L.X. Pang, J. Guo, Z.M. Qi, T. Shao, Q.P. Wang, H.D. Xie, X. Yao, C.A. Randall, Influence of Ce Substitution for Bi in $BiVO_4$ and the impact on the phase evolution and microwave dielectric properties, Inorg. Chem. 53 (2014) 1048–1055.
[3] D. Zhou, L.X. Pang, J. Guo, Z.M. Qi, T. Shao, X. Yao, C.A. Randall, Phase evolution, phase transition, and microwave dielectric properties of scheelite structured $xBi(Fe_{1/3}Mo_{2/3})O_4$-$(1-x)BiVO_4$ ($0.0 \le x \le 1.0$) low temperature firing ceramics, J. Mater. Chem. 22 (2012) 21412–21419.
[4] A. Baumgarte, R. Blachnik, New $M^{2+}M^{4+}Nb_2O_8$ phases, J. Alloys Compd. 215 (1994) 117–120.
[5] Q.W. Liao, L.X. Li, X. Ren, X. Ding, New low-loss microwave dielectric material $ZnTiNbTaO_8$, J. Am. Ceram. Soc. 94 (2011) 3237–3240.
[6] Q.W. Liao, L.X. Li, X. Ren, X.X. Yu, Q.L. Meng, W.S. Xia, A new microwave dielectric materials $Ni_{0.5}Ti_{0.5}NbO_4$, Mater. Lett. 89 (2012) 351–353.
[7] C.L. Huang, S.H. Huang, R.Z. Lee, The microwave dielectric materials of $(Zn_{1-x}Mg_x)TiNb_2O_8$ for electroceramics devices applications, Key Eng. Mater. 547 (2013) 49–55.
[8] Q.W. Liao, L.X. Li, P. Zhang, L.F. Cao, Y.M. Han, Correlation of crystal structure and microwave dielectric properties for $Zn(Ti_{1-x}Sn_x)Nb_2O_8$ ceramics, Mater. Sci. Eng. B 176 (2011) 41–44.
[9] Q.W. Liao, L.X. Li, X. Ren, X.X. Yu, D. Guo, M.J. Wang, A low sintering temperature low loss microwave dielectric material $ZnZrNb_2O_8$, J. Am. Ceram. Soc. 95 (2012) 3363–3365.
[10] Y. Cheng, R.Z. Zuo, Y. Lv, Preparation and microwave dielectric properties of low-loss $MgZrNb_2O_8$ ceramics, Ceram. Int. 39 (2013) 8681–8685.
[11] S.D. Ramarao, V.R.K. Murthy, Crystal structure refinement and microwave dielectric properties of new loss dielectric loss $AZrNb_2O_8$ (A: Mn, Zn, Mg and Co) ceramics, Scr. Mater 69 (2013) 274–277.
[12] X. Tang, H. Yang, Q.L. Zhang, J.H. Zhou, Low-temperature sintering and

microwave dielectric properties of $ZnZrNb_2O_8$ ceramics with $BaCu(B_2O_5)$ addition, Ceram. Int. 40 (2014) 12875–12881.
[13] C.L. Huang, J.Y. Chen, Y.W. Tseng, C.Y. Jiang, G.S. Huang, High dielectric constant and low-loss microwave dielectric ceramics using $(Zn_{0.95}M^{2+}{}_{0.05})Ta_2O_6$ (M2+=Mn, Mg, and Ni) solid solutions, J. Am. Ceram. Soc. 93 (2010) 3299–3304.
[14] W.S. Xia, L.X. Li, L.J. Ji, P. Zhang, P.F. Ning, Q.W. Liao, Phase evolution, bond valence and microwave characterization of $(Zn_{1-x}Ni_x)Ta_2O_6$ ceramics, Mater. Lett. 66 (2012) 296–298.
[15] T.K. Chen, W.B. Ma, R. Li, Q.C. Sun, C.C. Tang, Z.L. Huan, Phase composition and microwave dielectric properties of (Zn, Ni)$TiNb_2O_8$ solid solution, J. Mater. Sci. 25 (2014) 2494–2500.
[16] B.W. Hakki, P.D. Coleman, A dielectric resonator method of measuring inductive capacities in the millimeter range,, IEEE Trans. Microw. Theory Tech. 8 (1960) 402–410.
[17] W.E. Courtney, Analysis and evaluation of a method of measuring the complex permittivity and permeability microwave insulators, IEEE Trans. Microw. Theory Tech. 18 (1970) 476–485.
[18] E.S. Kim, B.S. Chun, R. Freer, R.J. Cernik, Effects of packing fraction and bond valence on microwave dielectric properties of $A^{2+}B^{6+}O_4$ (A^{2+}: Ca, Pb, Ba; B^{6+}: Mo, W) ceramics, J. Eur. Ceram. Soc. 30 (2010) 1731–1736.
[19] L. Glasser, H.D.B. Jenkins, Lattice energy and unit cell volumes of complex ionic solids, J. Am. Chem. Soc. 122 (2000) 632–638.
[20] K.M. Manu, C. Karthik, R. Ubic, M.T. Sebastian, Effect of Ca^{2+} substitution on the structure, microstructure, and microwave dielectric properties of $Sr_2Al_2SiO_7$ ceramic, J. Am. Ceram. Soc. 96 (2013) 3842–3848.
[21] R.D. Shannon, Dielectric polarizabilities of ions in oxides and fluorides, J. Appl. Phys. 71 (1993) 348–366.
[22] P.J. Harrop, Temperature coefficients of capacitance of solids, J. Mater. Sci. 4 (1969) 370–374.
[23] S.R. Kiran, G. Sreenivasulu, V.R.K. Murthy, V. Subramanian, B.S. Murty, Effects of grain size on the microwave dielectric characteristics of high-energy ball-milled zinc magnesium titanate ceramics, J. Am. Ceram. Soc. 95 (2012) 1973–1979.